West Pacific and ENSO Seasonality Driven by the South Asian Monsoon

P.J. Tuckman[1*], Jane E. Smyth[1], Jingyuan Li[2], Nicholas Lutsko[2], John Marshall[1]

[1]Department of Earth, Atmospheric, and Planetary Sciences, Massachusetts Institute of Technology, 21 Ames Street, Cambridge, 02142, Massachusetts, United States.
[2]Scripps Institution of Oceanography, University of California, San Diego, 8622 Kennel Way, La Jolla, 92037, California, United States.

*Corresponding author(s). E-mail(s): ptuckman@mit.edu;
Contributing authors: jane.smyth@man.com; jil308@ucsd.edu; nlutsko@ucsd.edu; jmarsh@mit.edu;

Abstract

The Equatorial Pacific and ENSO have climatologically important seasonal cycles, with maximum Western Pacific SSTs occurring during boreal autumn and ENSO events peaking during boreal winter. In this work, we use the concept of a monsoonal mode to show that the presence of a large landmass in the northern hemisphere leads to this seasonal cycle. Specifically, warm air moving east from the Asian summer monsoon suppresses surface fluxes in the West Pacific, leading to increased heat content there during the following months. This, in turn, enhances ENSO growth rates during boreal autumn and causes ENSO events to peak in boreal winter.

Keywords: Pacific warm pool, Seasonal cycle, ENSO, Monsoonal Mode

1 Introduction

The equatorial Pacific can be divided into two parts: a West Pacific warm pool and an East Pacific cold tongue. The interannual variability of the East Pacific, and much of the world, is dominated by the El Niño-Southern Oscillation (ENSO), characterized by warming of the Central and Eastern Equatorial Pacific. Both the West Pacific and ENSO have seasonal cycles which favor one season, despite insolation on the equator peaking twice a year. The equatorial West Pacific (Fig. 1a) is at a roughly constant temperature through June-July-August (JJA), then warms during September-October-November (SON), cools very quickly during December-January-February (DJF), and warms again during March-April-May (MAM). If this temperature were controlled only by incoming solar radiation, it would have two maxima over the course of the year, yet it has only one. The seasonal asymmetry of the equatorial Pacific can also be seen by comparing October and April; in October the West Pacific is warmer than in April, while the East Pacific is colder (Fig. 1b). This asymmetry affects the seasonality of ENSO, despite it being an interannual phenomenon with a period of 3-6 years. For example, the 1997-1998 El Niño event had a clear signal in June (c), but strengthened considerably during SON and peaked in December (d). Almost all ENSO events, both positive and negative, peak during DJF (e); of the nine largest ENSO peaks between 1959-2021, seven occurred in December or January, and none occurred in JJA.

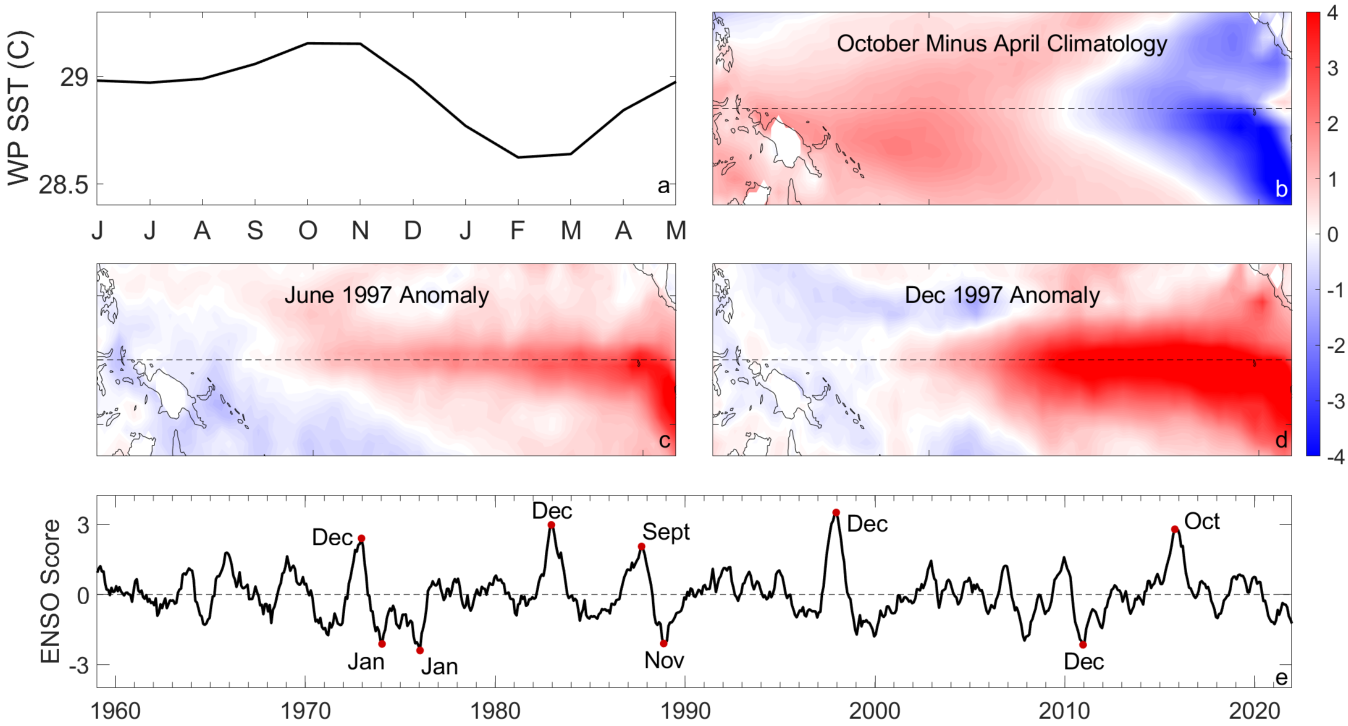

Fig. 1 (a) The seasonal cycle of West Pacific SST (160-190°E, 15°N-15°S), (b) the difference in SST between the October and April climatology (zonal mean removed), and (c) June and (d) December SST anomalies during the growth of the 1997 El Niño event. (e) A detrended time series of ENSO score, defined as the first principal component of interannual variability of tropical SSTs. The months of the positive and negative peaks of normalized amplitude larger than two are labelled.

The West Pacific warm pool and its seasonality have been studied extensively [1–8], with previous research identifying net surface heat flux [9, 10] and wind-forced Kelvin and Rossby waves [11] as controlling tropical SSTs on seasonal time-scales. However, the cause of the spring/autumn asymmetry in the equatorial West Pacific has not been explained.

The tropical Pacific is of outsized importance in global climate due to ENSO [12–15], which impacts worldwide weather [16–18] and SSTs [19]. Previous work on ENSO, using methods ranging from simplified analytic models [e.g., 20, 21] to intermediate complexity models [e.g., 22] and full general circulation models (GCMs) [e.g., 23–26], has found that ENSO's seasonality is set by El Niño growth rates, which are largest during SON [27–30]. Tziperman et al. [31] showed, using the Zebiak and Cane ENSO model [32], that these growth rates are controlled by the wind divergence and background SSTs of the equatorial Pacific. In other words, it has been shown that the climatological seasonality of the Pacific plays a critical role in the phasing of ENSO [33], but our understanding of the seasonality of the Equatorial Pacific remains incomplete.

This study demonstrates the role of the Asian monsoon in the seasonality of ENSO. We use the concept of the Indo-Pacific monsoonal mode introduced in Tuckman et al. [34] as a framework: warm air moving east from Asia during JJA suppresses surface fluxes in the West Pacific, enhancing SSTs, and therefore the temperature gradient across the Pacific, during SON. This strengthens the Walker circulation, creating a seasonality in the low level winds, which, together with that of SSTs, phase-locks ENSO to the seasonal cycle. We run idealized coupled simulations with two simplified continental configurations, one with a representation of Asia and one without. Only in the presence of Asia, and therefore a monsoon, do the equatorial Pacific and ENSO have seasonal cycles that match reanalysis.

2 Pacific Seasonality with and without a Monsoon

We use coupled atmosphere-ocean MITgcm experiments (details in Methods) and ERA5 atmospheric reanalysis [35], to explore Asia's role in the seasonality of the equatorial Pacific. The coupled models (Fig. 2, left) have thin barriers which separate the ocean into basins, and the "continent" simulation represents Asia as a region with reduced heat capacity and no ocean dynamics. This leads to intense precipitation during JJA, analogous to the South Asian Monsoon, while the "aquaplanet" simulation has no representation of land, and therefore no monsoon.

In simulations with and without a continent, the first principal component of interannual variability in tropical ocean temperatures resembles the observed ENSO mode (Fig. 2, right column). This mode shows warming of the central and eastern equatorial Pacific, cooling of the Western Pacific, and explains 25%-35% of interannual variability in the tropics. The regions to be studied are highlighted with orange (West Pacific) and blue boxes (East Pacific). We analyze potential temperature at 25 meters depth (hereafter θ_{25}) for the simulations as it is less noisy and a better metric of ocean heat content than SST, while for reanalysis we use SST as it is the most readily available variable. Additionally, the simulations have irrelevant upwelling along the eastern boundary of the Pacific which affects the SST, but not θ_{25}. The simulations' ENSO modes have roughly similar periods to the observed ENSO (bottom of Fig. 2) whose broad power spectrum peaks at roughly 4 years. The modeled power spectra peak at 4 years (aquaplanet) and 5 years (continent): both are within the error bounds of the observed power spectrum. The difference in the period of ENSO between the simulations could be due to the presence of a continent influencing teleconnections between the Indian and Pacific Oceans, but it is not our focus here.

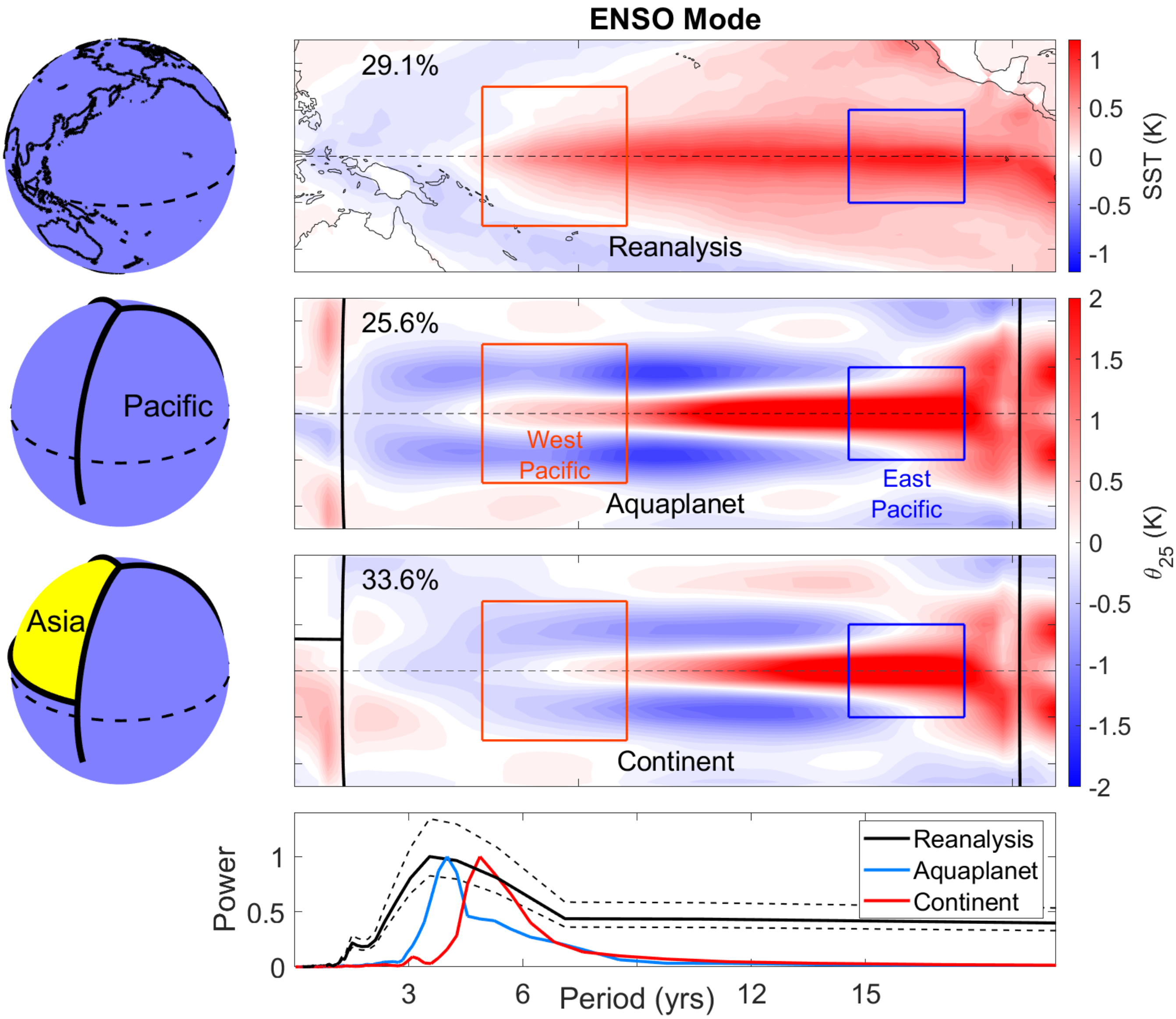

Fig. 2 (left) Continental configuration and (right) the ENSO mode, calculated as the first principal component of interannual variability for (top) reanalysis data, (middle) the "aquaplanet" simulation, and (bottom) the "continent" simulation. Asia reaches from 0° to 135°E and from 8° to 90°N in the continent simulation, and the thin barriers are at 0°E, 135°, and 270°E in both simulations. The fraction of variability explained is shown in the top left of each panel. (bottom) The power spectra of the ENSO mode in each case, with a 50% confidence interval plotted as thin dashed lines for reanalysis. Rectangular boxes indicate regions which are representative of the West Pacific (orange, 160-190°E, 15°N-15°S) and East Pacific (blue, 240-265°E, 10°N-10°S). The ENSO mode is calculated from reanalysis SSTs and from potential temperature 25 meters below the surface (θ_{25}) in the simulations.

The seasonality of the equatorial Pacific is well reproduced in the continent simulation (Fig. 3). In the West Pacific (panel a), reanalysis SSTs peak in SON and have a minimum in February. The θ_{25} from the continent simulation is comparable, peaking in October and November and having a minimum in February and March. The aquaplanet simulation, however, has a roughly symmetric seasonal cycle, with maxima during both solstitial seasons. Without a continent to break hemispheric symmetry, there is little difference between summer and winter along the equator. Note that there is a systematic bias in the simulations towards a larger seasonal cycle of temperature, likely due to model idealizations such as a lack of clouds and atmospheric shortwave absorption, a simple ocean mixing scheme, and biases in ocean mixed layer depth.

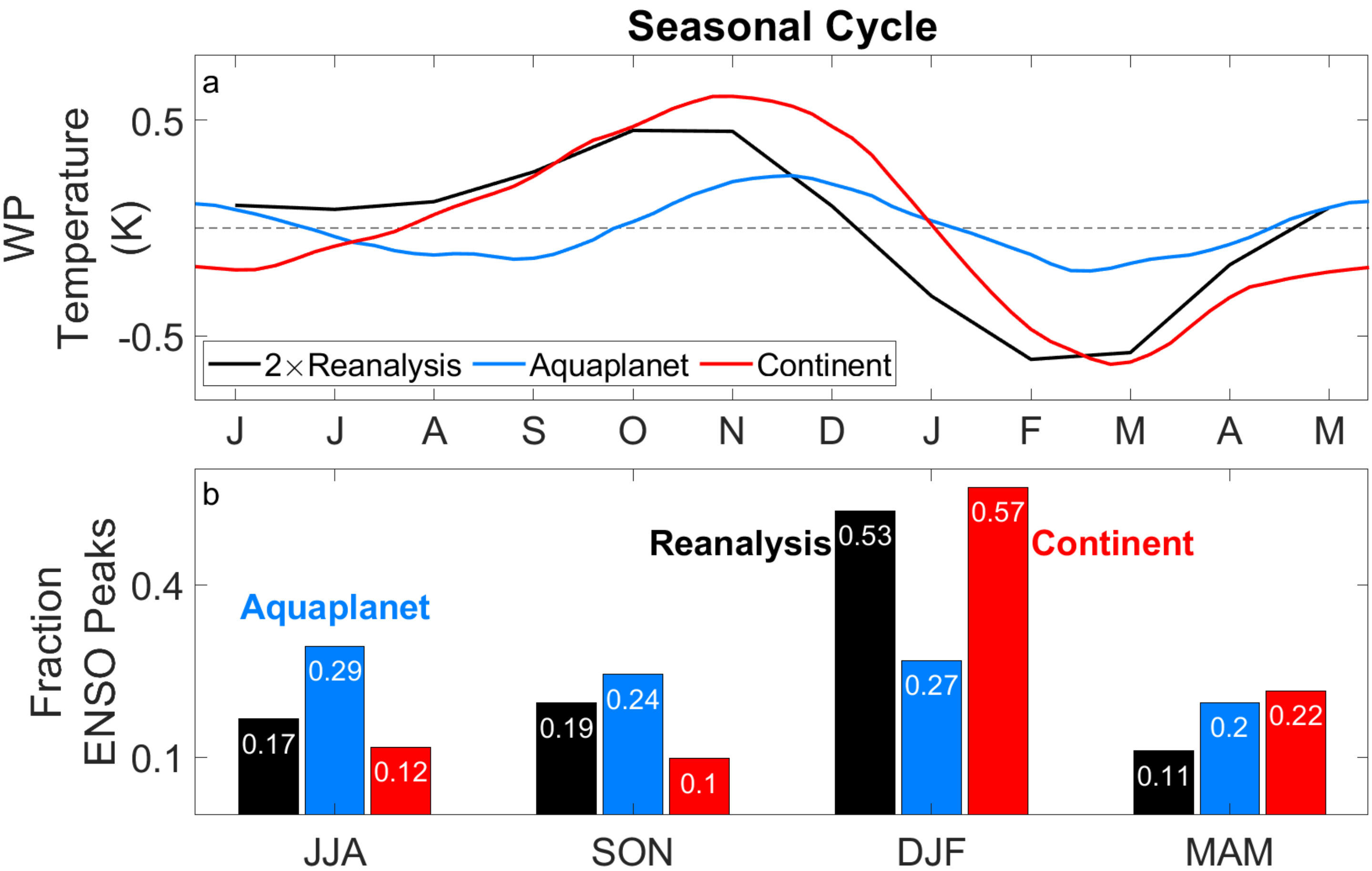

Fig. 3 The seasonality of the equatorial Pacific. Panel a shows the seasonal cycle of West Pacific reanalysis SST (black) and potential temperature 25 meters below the surface (θ_{25}) from the aquaplanet simulation (blue) and continent simulation (red). Panel b shows the fraction of ENSO peaks that occur in each season for reanalysis (black), the aquaplanet simulation (blue), and the continent simulation (red). The reanalysis SST in panel a is multiplied by two so that the amplitude is similar to that of θ_{25} from the continent simulation.

Next, we compare the seasonal distribution of ENSO peaks in observations to that of the simulations (Fig. 3b). An ENSO peak is defined as when the East Pacific temperature is 1.5 standard deviations (1 in reanalysis, since it is a shorter time series) away from the mean for that season and is at its most extreme within a 12 month window. In reanalysis, more than half of ENSO peaks occur in DJF, while 17% occur during JJA. ENSO seasonality in the continent simulation is similar, with almost 60%

of peaks being during DJF, and 12% in JJA. In the aquaplanet simulation, however, there is little seasonality, with between 20% and 30% of peaks occurring in each season.

In summary, the continent simulation broadly captures the seasonality of the equatorial Pacific, both in its climatology and interannual variability, while the aquaplanet simulation does not. This strongly suggests that the presence of Asia plays an important role in the Pacific's seasonality, which we now explain using the concept of a monsoonal mode.

2.1 Role of the Monsoonal Mode

In observations, an atmospheric energy and precipitation anomaly forms over South Asia in northern spring/summer due to heating over land, is advected eastwards into the West Pacific in northern autumn, and remains there due to interactions with the Pacific cold tongue and equatorial easterlies. In Tuckman et al. [34] we interpret this phenomenon as a "monsoonal mode," a zonally propagating moist energy anomaly of continental and seasonal scale. This provides a framework for how the monsoon influences the seasonal cycle of the West Pacific and ENSO (Fig. 4). The monsoonal mode is most clearly visible in the seasonality of the energy flux potential (EFP, defined in Methods) [36], a measure of atmospheric energy transport. Fig. 4 shows the seasonal cycle of the EFP maxima, the region from which atmospheric energy is exported meridionally and zonally in (a) reanalysis, (b) the aquaplanet simulation, and (c) the continent simulation. In the continent simulation and reanalysis, energy is exported from Southern Asia/the Northern Indian Ocean during JJA and from the equatorial West Pacific during DJF. In the aquaplanet simulation, a warm pool in the Western Indian Ocean leads to a small EFP maximum there with little seasonal movement. With no continent, the movement of the EFP maximum is controlled by solar radiation and the Indian Ocean cold tongue.

When there is a continent (Fig.4d, grey), it is very warm during JJA due to its low heat capacity, leading to large energy fluxes from the land surface (orange arrows), and an EFP maximum (green circle). The warm air above the continent is advected eastward by the monsoon winds (black arrow), leading to anomalously warm air over a cool surface. This suppresses surface fluxes (red arrows), leading to less energy leaving the West Pacific in the continent simulation than the aquaplanet simulation during JJA and September (panel e). Consequently, the West Pacific is warmer in the continent simulation during SON (panel f). In summary, warm air moving east from Asia during JJA suppresses surface fluxes in the West Pacific, causing ocean heat content there to peak in SON, as seen in Fig. 3a.

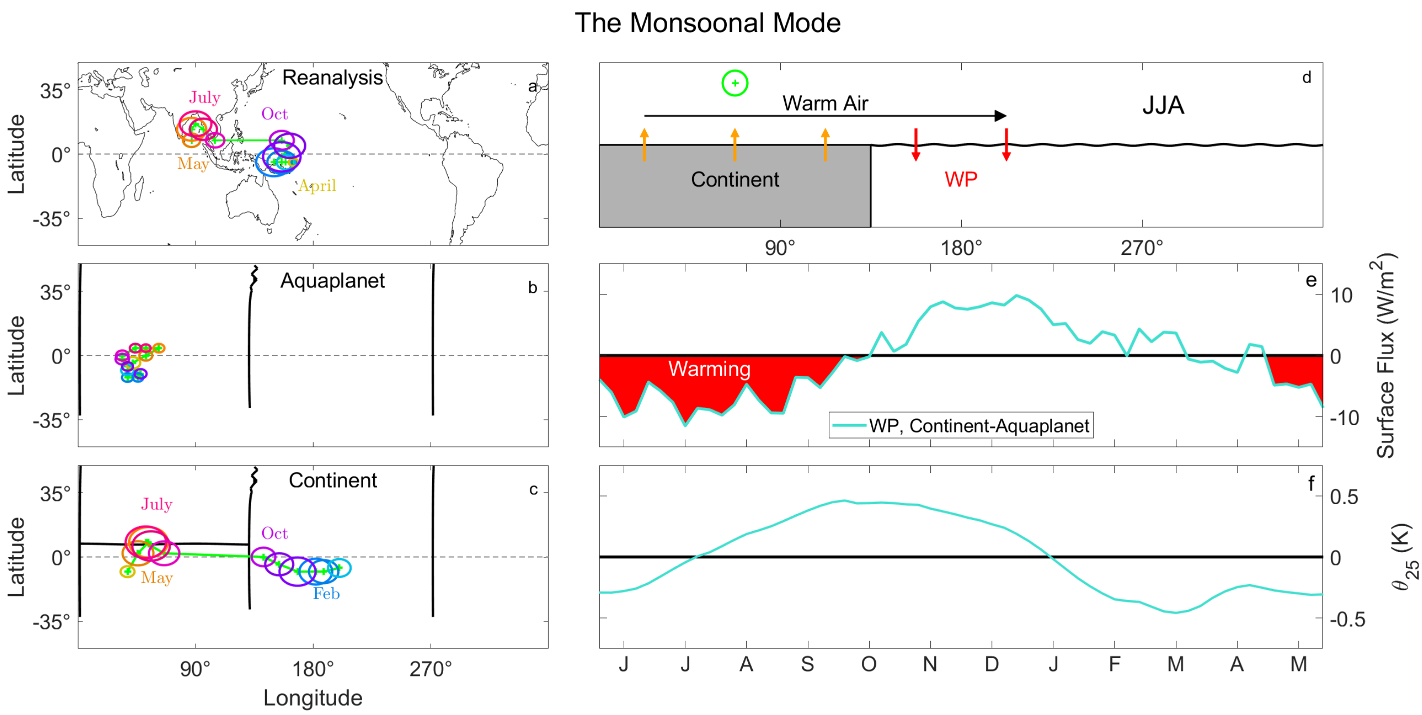

Fig. 4 Elements of the monsoonal mode. The seasonal cycle of the energy flux potential maximum in (a) reanalysis, (b) the aquaplanet and (c) the continent simulations. The color of the circle changes each month, and its radius is a measure of the strength of zonal heat transport. The monthly positions of the EFP maxima are shown by green crosses and connected with a green line (in panels a and c). (d) A schematic of the monsoonal mode in JJA. (e) The difference in West Pacific surface flux between the continent and aquaplanet simulations over the seasonal cycle. (f) The difference in West Pacific θ_{25} between the continent and aquaplanet simulations.

2.2 Seasonality of ENSO

To explore the processes influencing ENSO seasonality, we study the temperature of the near-surface equatorial central and eastern Pacific (190°-265°E, 20-40 meters depth). This region is chosen to monitor anomalous temperature of the East Pacific, but extends into the Central Pacific so that ENSO seasonality can be directly related to the monsoonal mode through the West Pacific temperature. We evaluate a regionally averaged linearized anomalous temperature budget:

$$\frac{1}{T'}\frac{\partial}{\partial t}T' \approx -\frac{\Delta_x T'}{T'}\bar{U} - \frac{U'}{T'}\Delta_x \bar{T} - \frac{\Delta_z T'}{T'}\bar{W} - \frac{W'}{T'}\Delta_z \bar{T}, \tag{1}$$

where T is temperature, U is the zonal current, and W is the vertical current. Overbars denote the climatological seasonal cycle, primes denote anomalies, and Δ_x and Δ_z indicate finite differences in the zonal and vertical directions. We neglect nonlinear terms, meridional advection, and anomalous sources or sinks (further details can be found in Methods). Each term has been divided by T' so that it can be interpreted as contributions to a growth rate with units of 1/time (schematic on left side of Fig. 5).

The seasonal contributions of each term to the ENSO growth rates are shown on the right side of Fig. 5 for the continent (top) and aquaplanet simulations (bottom). The total growth rate for the continent simulation (black bars) is positive in JJA, peaks in SON, and is negative in DJF and MAM. It is primarily set by the mean zonal current acting on the anomalous temperature (orange), but has a contribution from the anomalous zonal current acting on the mean temperature (purple). These two terms are strongly influenced by the presence of a continent via the monsoonal mode. The horizontal temperature gradient ($\Delta_X \bar{T}$) across the Pacific increases between JJA and SON because the West Pacific is warmed by suppressed surface fluxes in JJA. Meanwhile, the mean zonal current ($\bar{U}$) is controlled by the strength of the Walker Circulation, which in turn is driven by the temperature gradient across the Pacific [37]. In the continent simulation, ascent is strong over the continent during JJA and over the West Pacific during SON, leading to a stronger Walker circulation and stronger zonal currents during those seasons. In the aquaplanet simulation (bottom right of Fig. 5), none of these terms have a large seasonal cycle, leading to little seasonality in ENSO peaks (Fig. 3).

Enhanced ENSO growth rates during JJA and SON in the continent simulation lead to ENSO events peaking during DJF, as this is when growth switches to decay. Therefore, the seasonality of ENSO is a consequence of the seasonal cycle of the zonal current (controlled by the Walker Circulation) and the zonal temperature gradient. These quantities are sensitive to the presence of a continent north of the equator, through the monsoonal mode warming the West Pacific and modulating the seasonality of the Walker circulation. These results are in agreement with Tziperman et al. [31], who found that the seasonal cycles of wind and SST control ENSO seasonality. Here, we have demonstrated that those seasonal cycles are controlled by the South Asian monsoon.

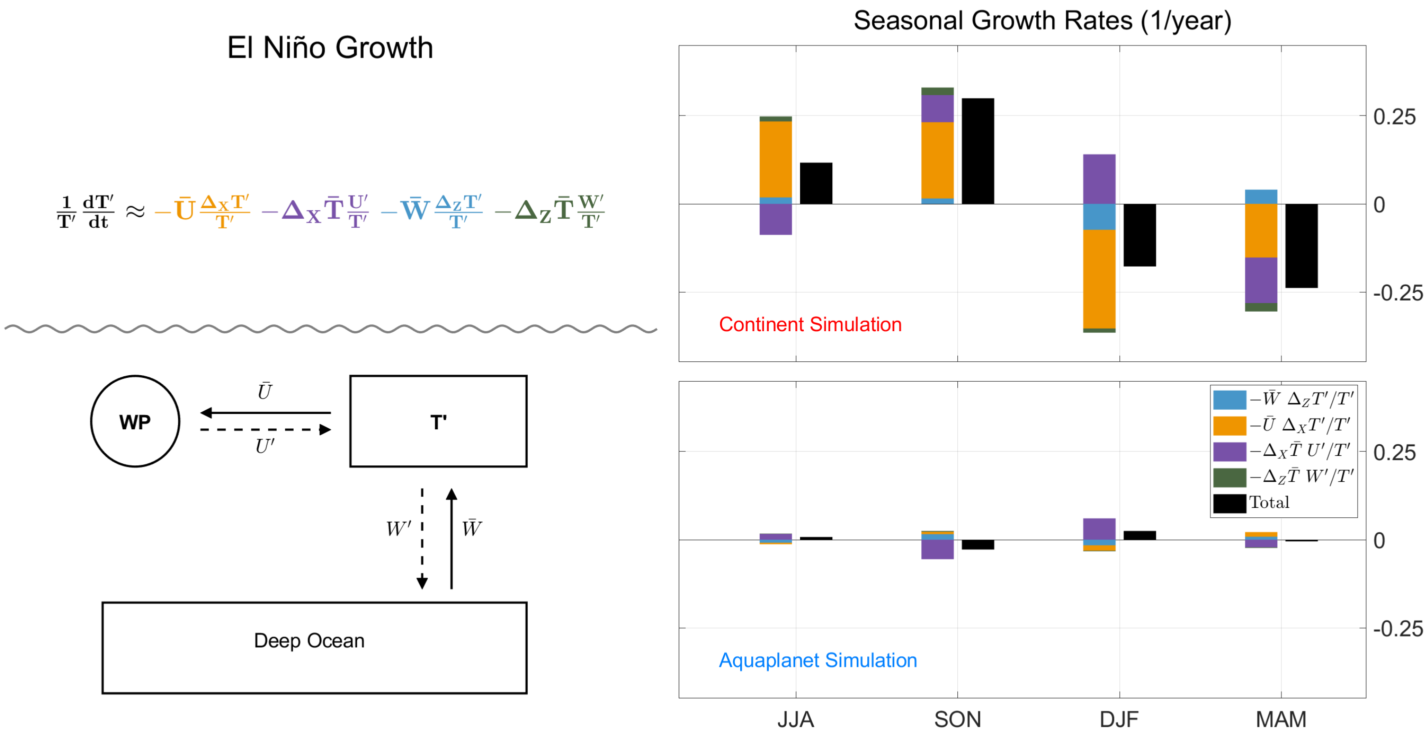

Fig. 5 Exploring processes that control simulated ENSO growth rates over the seasonal cycle. The left side shows a schematic of the Central-East Pacific (190°-265°E) energy budget and terms contributing to it. Arrows indicate current direction, overbars and solid arrows indicate the climatological seasonal cycle, while primes and dashed arrows indicate anomalies. The right side shows the seasonality of growth rates in the (top) continent and (bottom) aquaplanet simulations: the black bar is the total growth rate and its components are in colors. All growth terms are computed as the difference from the annual mean. Note that the total growth rate includes contributions from meridional advection, which are not shown directly here. More details can be found in Methods.

3 Discussion

We have proposed, and illustrated through numerical experiment and observations, a simple explanation for the seasonality of the equatorial Pacific and the seasonal phase-locking of ENSO. That the West Pacific is warmest during SON, and that ENSO events peak during DJF, can both be understood as consequences of the annual Indo-Pacific monsoonal mode, in which warm air moving eastward from the Asian Monsoon suppresses surface fluxes in the West Pacific [34]. In our aquaplanet simulation, which does not have a continent or a monsoon, the West Pacific has very little spring/autumn asymmetry, and ENSO events peak during JJA just as often as in DJF. However, when a monsoon is present, the West Pacific is warmest during SON and ENSO events peak during DJF, just as in observations. The seasonality of ENSO stems from the impact of the monsoonal mode on the Walker Circulation and the zonal temperature gradient across the Pacific.

Our study shows that the presence of Asia and its annual monsoon is a sufficient condition to capture the major seasonal asymmetries in the equatorial Pacific. However, it may not be a necessary condition, as there are other sources of hemispheric asymmetry on Earth. These include the Andes [38–40], the Atlantic Meridional Overturning Circulation [41], the precession of Earths orbit [42], and the slant of South America [43, 44], all of which may break the seasonal symmetry of the equatorial Pacific. Specifically, models have shown that the North-East slant of South America enhances nearby eastward surface currents, and therefore upwelling, when the tropical winds are southerly during JJA and SON [43]. However, the influence of the monsoon considered here is a more intuitive explanation of ENSO seasonality, is consistent with previous work [31], and incorporates an understanding of the spring/autumn asymmetry in the West Pacific.

Our results have important implications for understanding the equatorial Pacific. First, they directly relate tropical Pacific behavior to that of Asia and the monsoon. This means that studying the equatorial Pacific requires consideration of possible influences of the monsoonal mode. Here, we have mostly discussed seasonal timescales, but the interannual variability of the monsoon, and the modulation of the monsoonal mode by different continental configurations of the past, will also influence the equatorial Pacific. The connection between the Monsoon and ENSO also suggests a framework in which to analyze biases in model representations of ENSO. Specifically, model biases in ENSO seasonality [45–47] may be due to inadequate representations of Asia or of the Asian monsoon.

Second, any insight into ENSO seasonality may have implications for the spring predictability barrier (SPB) [48, 49]. The ENSO state helps initialize seasonal predictions, so negative ENSO growth rates in MAM make it hard to predict the climate in the following months. It has been previously hypothesized that monsoon forcing plays a role in the SPB [50], but through monsoon variability, rather than modulation of ENSO growth rates. The framework of the monsoonal mode suggests a simple and intuitive reason for the SPB: negative ENSO growth rates in the spring, which are caused by a weakened Walker Circulation and a small zonal temperature gradient across the Pacific, are due to the presence of a large continent in the Northern Hemisphere. By connecting the seasonality of ENSO to the presence of Asia, we have made progress towards understanding the fundamental predictability of the Earth system.

4 Methods

In this section, we discuss the coupled simulations used, the calculation of the energy flux potential shown in Fig. 4, the use of reanalysis data, and the ENSO energy budget discussed in reference to Fig. 5.

Coupled Model Simulations

The coupled atmosphere-ocean simulations used in this study are similar to those described in Tuckman et al. [34] based on the MITgcm [51]. The code is available at https://github.com/MITgcm/verification_other/tree/master/cpl_gray%2Bswamp%2Bocn. Simulations are run for at least 750 years to ensure that the coupled system achieves a quasi-steady state. Diagnostics are averaged over the final 100 years, except in the calculation of ENSO statistics (i.e., Fig. 2), which uses 200 years to minimize noise.

The model employs identical cubed-sphere grids representing the atmosphere and ocean with $\sim 2.8°$ horizontal resolution in the tropics [52]. The atmosphere has 26 vertical levels, idealized moist physics, a gray radiation scheme [53], and water vapor feedback on longwave optical thickness [54]. There are no clouds or shortwave absorption in the atmosphere. The model employs a seasonal cycle of solar radiation appropriate for a circular orbit with an obliquity of 23.45°.

The dynamic ocean has 38 vertical levels with a uniform depth of 3.4 km, and uses the mixing scheme developed in Gaspar et al. [55]. The continent simulation has three infinitesimally thin ridges running south from the North Pole and a large landmass, treated as a 2m slab ocean (globe in Fig. 2), extending from roughly 8°N to the North Pole. The landmass represents Asia, two thin barriers stretching from the North Pole to 35°S demarcate the Atlantic basin, and one reaching 30°S separates the Indian and Pacific oceans. In order to conserve freshwater, excess water that precipitates over the continent is redirected into the Atlantic basin. The aquaplanet simulation has the same three North-South boundaries, but has no representation of Asia.

Both simulations have a West Pacific warm pool and an East Pacific cold tongue comparable to reanalysis, despite the highly idealized model. The simulated surface winds exhibit an Inter-Tropical Convergence Zone, tropical easterlies, and extratropical westerlies (as shown in Tuckman et al. [34], Fig. 3). It should be noted that the simulations' ENSO patterns feature a negative signal in the equatorial Atlantic, and the aquaplanet has a positive signal in the equatorial Indian ocean (not shown). This is likely due to ENSO teleconnections between basins that are delineated by thin barriers. This is not of relevance to our focus here.

The Energy Flux Potential and Reanalysis Data

We calculate an energy flux potential χ [36], which is a solution to:

$$\nabla^2 \chi = -\vec{\nabla} \cdot \langle h\vec{u} \rangle, \tag{2}$$

where ∇^2 is the 2D Laplacian acting on a scalar, $\vec{\nabla}\cdot$ is the 2D divergence, and $\langle h\vec{u} \rangle$ is the vertically integrated horizontal transport of moist static energy (MSE), defined as:

$$h = Lq + gz + c_p T, \tag{3}$$

where q is specific humidity, z is height, T is temperature, and the constants $L \equiv 2.25 \times 10^3$ kJ/kg, $g \equiv 9.8$ m/s^2, and $c_p \equiv 1005$ J/kg/K are the latent heat of vaporization of water, the acceleration due to gravity, and the specific heat of air at constant pressure.

We use monthly means from the ERA5 global atmospheric reanalysis produced by ECMWF [35] and the mass corrected divergence of total energy [56]. The divergence includes a component from kinetic energy, although this contribution is negligible compared to the moist static energy described above. The EFP data are averaged from 1979-2020 to calculate climatological means, while the SST data are averaged from 1959-2021.

Energy budget and ENSO Growth Rates

We use an ocean energy budget applied to the Central-Eastern Pacific to understand how the growth of ENSO is modulated by the seasonal cycle. We write an ocean temperature budget:

$$\frac{\partial}{\partial t}T + U\frac{\partial}{\partial x}T + V\frac{\partial}{\partial y}T + W\frac{\partial}{\partial z}T = S_i - S_o \tag{4}$$

where T is the temperature as a function of position (x,y,z) and time (t), temperature is advected by the currents (U,V,W), and source and sink terms are summarized as S_i and S_o, respectively. We focus on the near-surface equatorial central and eastern Pacific (190°-265°E, 20-40 meters depth). This is chosen to monitor the anomalous temperature of the East Pacific, but extends through the Central Pacific so that ENSO seasonality can be directly related to the monsoonal mode through the West Pacific temperature.

Terms are evaluated using finite differences to approximate the spatial derivatives, and the temperature budget can then be written:

$$\frac{\partial}{\partial t}T + U\Delta_x T + V\Delta_y T + W\Delta_z T = S_i - S_o$$

where all quantities are averaged over our chosen region. We now split each term (e.g., T) into a climatological seasonal cycle ($\bar{T}$) and an anomaly from this seasonal cycle (T') yielding a temperature budget for the mean seasonal cycle:

$$\frac{\partial}{\partial t}\bar{T} = -\bar{U}\Delta_x\bar{T} - \bar{V}\Delta_y\bar{T} - \bar{W}\Delta_z\bar{T} + \bar{S}_i - \bar{S}_o$$

and anomalies from it:

$$\begin{aligned}\frac{\partial}{\partial t}T' = &-\bar{U}\Delta_x T' - U'\Delta_x\bar{T} - U'\Delta_x T' \\ &-\bar{V}\Delta_y T' - V'\Delta_y\bar{T} - V'\Delta_y T' \\ &-\bar{W}\Delta_z T' - W'\Delta_z\bar{T} - W'\Delta_z T' \\ &+ S_i' - S_o'.\end{aligned}$$

We are interested in how an El Niño anomaly, i.e., a positive value of T', is influenced by the climatological seasonal cycle, i.e., $\bar{T}$, $\bar{U}$, $\bar{V}$, and $\bar{W}$. The relevant terms are therefore the ones that are the product of a mean and an anomaly quantity, such as $\bar{U}\Delta_x T'$, $U'\Delta_x\bar{T}$ etc. Previous work has shown that the relevant terms for the growth of El Niño events, especially with regards to the seasonal cycle, are the zonal and vertical advection [31, 33, 57], supporting the neglect of source and sink terms. We also neglect meridional advection since its contribution is small.

Four terms remain: 1. The mean horizontal current acting on the anomalous temperature, 2. the anomalous horizontal current acting on the mean temperature, 3. the anomalous vertical current acting on the mean temperature, and 4. the mean vertical current acting on the anomalous temperature. Dividing by T' to obtain quantities with units of inverse time (i.e. a growth rate), we can write:

$$\frac{1}{T'}\frac{\partial}{\partial t}T' = -\frac{\Delta_x T'}{T'}\bar{U} - \frac{U'}{T'}\Delta_x \bar{T} - \frac{\Delta_z T'}{T'}\bar{W} - \frac{W'}{T'}\Delta_z \bar{T}. \quad (5)$$

This expression comprises four terms which are evaluated and then composited over 6 El Niño peaks, averaging from 1.5 months before to 1.5 months after each peak. The resulting growth rates are shown in Fig. 5, with meridional advection terms included in the total growth rate for completeness.

Acknowledgments. P.J. Tuckman, J. Li, J. Marshall, and N. Lutsko are supported by NSF grant OCE-2023520. J. Smyth was supported by the NSF atmospheric and geospace sciences postdoctoral research fellowship (award no. 2123372). We thank Jean-Michel Campin for his modeling contributions to this work.

References

[1] Köberle, C., Philander, S.G.H.: On the processes that control seasonal variations of sea surface temperatures in the tropical Pacific Ocean. Tellus A **46**(4), 481–496 (1994) https://doi.org/10.1034/j.1600-0870.1994.00011.x . _eprint: https://onlinelibrary.wiley.com/doi/pdf/10.1034/j.1600-0870.1994.00011.x. Accessed 2023-02-01

[2] DeWitt, D.G., Schneider, E.K.: The Processes Determining the Annual Cycle of Equatorial Sea Surface Temperature: A Coupled General Circulation Model Perspective. Monthly Weather Review **127**(3), 381–395 (1999) https://doi.org/10.1175/1520-0493(1999)127⟨0381:TPDTAC⟩2.0.CO;2 . Publisher: American Meteorological Society Section: Monthly Weather Review. Accessed 2023-03-07

[3] Schneider, E.K.: Understanding Differences between the Equatorial Pacific as Simulated by Two Coupled GCMs. Journal of Climate **15**(5), 449–469 (2002) https://doi.org/10.1175/1520-0442(2002)015⟨0449:UDBTEP⟩2.0.CO;2 . Publisher: American Meteorological Society Section: Journal of Climate. Accessed 2023-03-07

[4] Chang, P.: A study of the seasonal cycle of sea surface temperature in the tropical Pacific Ocean using reduced gravity models. Journal of Geophysical Research: Oceans **99**(C4), 7725–7741 (1994) https://doi.org/10.1029/93JC03561 . _eprint: https://onlinelibrary.wiley.com/doi/pdf/10.1029/93JC03561. Accessed 2023-02-01

[5] Clement, A.C., Seager, R., Murtugudde, R.: Why Are There Tropical Warm Pools? Journal of Climate **18**(24), 5294–5311 (2005) https://doi.org/10.1175/JCLI3582.1 . Publisher: American Meteorological Society Section: Journal of Climate. Accessed 2023-03-07

[6] Kim, S.T., Yu, J.-Y., Lu, M.-M.: The distinct behaviors of Pacific and Indian Ocean warm pool properties on seasonal and interannual time scales. Journal of Geophysical Research: Atmospheres **117**(D5) (2012) https://doi.org/10.1029/2011JD016557 . _eprint: https://onlinelibrary.wiley.com/doi/pdf/10.1029/2011JD016557. Accessed 2023-03-05

[7] Yin, Z., Dong, Q., Kong, F., Cao, D., Long, S.: Seasonal and Interannual Variability of the Indo-Pacific Warm Pool and its Associated Climate Factors Based on Remote Sensing. Remote Sensing **12**(7), 1062 (2020) https://doi.org/10.3390/rs12071062 . Number: 7 Publisher: Multidisciplinary Digital Publishing Institute. Accessed 2023-03-07

[8] Wang, Y., Wu, R., Wen, Z.: Seasonal variations in size and intensity of the Indo-western Pacific warm pool in different sectors. Journal of Oceanography **75**(5), 423–439 (2019) https://doi.org/10.1007/s10872-019-00511-y . Accessed 2023-03-07

[9] Wang, W., McPhaden, M.J.: The Surface-Layer Heat Balance in the Equatorial Pacific Ocean. Part I: Mean Seasonal Cycle. Journal of Physical Oceanography **29**(8), 1812–1831 (1999) https://doi.org/10.1175/1520-0485(1999)029⟨1812:TSLHBI⟩2.0.CO;2 . Publisher: American Meteorological Society Section: Journal of Physical Oceanography. Accessed 2023-03-07

[10] Schneider, N., Barnett, T., Latif, M., Stockdale, T.: Warm Pool Physics in a Coupled GCM. Journal of Climate **9**(1), 219–239 (1996) https://doi.org/10.1175/1520-0442(1996)009⟨0219:WPPIAC⟩2.0.CO;2 . Publisher: American Meteorological Society Section: Journal of Climate. Accessed 2023-03-07

[11] Yu, X., McPhaden, M.J.: Seasonal Variability in the Equatorial Pacific. Journal of Physical Oceanography **29**(5), 925–947 (1999) https://doi.org/10.1175/1520-0485(1999)029⟨0925:SVITEP⟩2.0.CO;2 . Publisher: American Meteorological Society Section: Journal of Physical Oceanography. Accessed 2023-03-07

[12] Philander, S.G.H., Yamagata, T., Pacanowski, R.C.: Unstable Air-Sea Interactions in the Tropics. Journal of the Atmospheric Sciences **41**(4), 604–613 (1984) https://doi.org/10.1175/1520-0469(1984)041⟨0604:UASIIT⟩2.0.CO;2 . Publisher: American Meteorological Society Section: Journal of the Atmospheric Sciences. Accessed 2023-04-11

[13] Battisti, D.S., Sarachik, E.S.: Understanding and predicting ENSO. Reviews of Geophysics **33**(S2), 1367–1376 (1995) https://doi.org/10.1029/95RG00933 . _eprint: https://onlinelibrary.wiley.com/doi/pdf/10.1029/95RG00933. Accessed 2023-02-02

[14] Clarke, A.J.: El Niño Physics and El Niño Predictability. Annual Review of Marine Science **6**(1), 79–99 (2014) https://doi.org/10.1146/annurev-marine-010213-135026 . _eprint: https://doi.org/10.1146/annurev-marine-010213-135026. Accessed 2023-04-19

[15] Timmermann, A., An, S.-I., Kug, J.-S., Jin, F.-F., Cai, W., Capotondi, A., Cobb, K.M., Lengaigne, M., McPhaden, M.J., Stuecker, M.F., Stein, K., Wittenberg, A.T., Yun, K.-S., Bayr, T., Chen, H.-C., Chikamoto, Y., Dewitte, B., Dommenget, D., Grothe, P., Guilyardi, E., Ham, Y.-G., Hayashi, M., Ineson, S., Kang, D., Kim, S., Kim, W., Lee, J.-Y., Li, T., Luo, J.-J., McGregor, S., Planton, Y., Power, S., Rashid, H., Ren, H.-L., Santoso, A., Takahashi, K., Todd, A., Wang, G., Wang, G., Xie, R., Yang, W.-H., Yeh, S.-W., Yoon, J., Zeller, E., Zhang, X.: El Niño–Southern Oscillation complexity. Nature **559**(7715), 535–545 (2018) https://doi.org/10.1038/s41586-018-0252-6 . Number: 7715 Publisher: Nature Publishing Group. Accessed 2023-02-01

[16] Neelin, J.D., Chou, C., Su, H.: Tropical drought regions in global warming and El Niño teleconnections. Geophysical Research Letters **30**(24) (2003) https://doi.org/10.1029/2003GL018625 . _eprint: https://onlinelibrary.wiley.com/doi/pdf/10.1029/2003GL018625. Accessed 2023-04-19

[17] Hoerling, M.P., Kumar, A., Zhong, M.: El Niño, La Niña, and the Nonlinearity of Their Teleconnections. Journal of Climate **10**(8), 1769–1786 (1997) https://doi.org/10.1175/1520-0442(1997)010⟨1769:ENOLNA⟩2.0.CO;2 . Publisher: American Meteorological Society Section: Journal of Climate. Accessed 2023-04-19

[18] Zhou, Z.-Q., Xie, S.-P., Zheng, X.-T., Liu, Q., Wang, H.: Global Warming–Induced Changes in El Niño Teleconnections over the North Pacific and North America. Journal of Climate **27**(24), 9050–9064 (2014) https://doi.org/10.1175/JCLI-D-14-00254.1 . Publisher: American Meteorological Society Section: Journal of Climate. Accessed 2023-04-19

[19] Johnson, G.C., Birnbaum, A.N.: As El Niño builds, Pacific Warm Pool expands, ocean gains more heat. Geophysical Research Letters **44**(1), 438–445 (2017) https://doi.org/10.1002/2016GL071767 . _eprint: https://onlinelibrary.wiley.com/doi/pdf/10.1002/2016GL071767. Accessed 2023-03-05

[20] Jin, F.-F.: A Simple Model for the Pacific Cold Tongue and ENSO. Journal of the Atmospheric Sciences **55**(14), 2458–2469 (1998) https://doi.org/10.1175/1520-0469(1998)055⟨2458:

ASMFTP⟩2.0.CO;2 . Publisher: American Meteorological Society Section: Journal of the Atmospheric Sciences. Accessed 2023-03-07

[21] Burgers, G., Jin, F.-F., Oldenborgh, G.J.: The simplest ENSO recharge oscillator. Geophysical Research Letters **32**(13) (2005) https://doi.org/10.1029/2005GL022951 . _eprint: https://onlinelibrary.wiley.com/doi/pdf/10.1029/2005GL022951. Accessed 2024-04-16

[22] Jin, F.-F., Kim, S.T., Bejarano, L.: A coupled-stability index for ENSO. Geophysical Research Letters **33**(23) (2006) https://doi.org/10.1029/2006GL027221 . _eprint: https://onlinelibrary.wiley.com/doi/pdf/10.1029/2006GL027221. Accessed 2023-02-07

[23] Philander, S.G.H., Pacanowski, R.C., Lau, N.-C., Nath, M.J.: Simulation of ENSO with a Global Atmospheric GCM Coupled to a High-Resolution, Tropical Pacific Ocean GCM. Journal of Climate **5**(4), 308–329 (1992) https://doi.org/10.1175/1520-0442(1992)005⟨0308:SOEWAG⟩2.0.CO;2 . Publisher: American Meteorological Society Section: Journal of Climate. Accessed 2023-02-27

[24] Guilyardi, E.: El Niño–mean state–seasonal cycle interactions in a multi-model ensemble. Climate Dynamics **26**(4), 329–348 (2006) https://doi.org/10.1007/s00382-005-0084-6 . Accessed 2023-03-07

[25] Guilyardi, E., Wittenberg, A., Fedorov, A., Collins, M., Wang, C., Capotondi, A., Oldenborgh, G.J.v., Stockdale, T.: Understanding El Niño in Ocean–Atmosphere General Circulation Models: Progress and Challenges. Bulletin of the American Meteorological Society **90**(3), 325–340 (2009) https://doi.org/10.1175/2008BAMS2387.1 . Publisher: American Meteorological Society Section: Bulletin of the American Meteorological Society. Accessed 2023-03-07

[26] Delecluse, P., Davey, M.K., Kitamura, Y., Philander, S.G.H., Suarez, M., Bengtsson, L.: Coupled general circulation modeling of the tropical Pacific. Journal of Geophysical Research: Oceans **103**(C7), 14357–14373 (1998) https://doi.org/10.1029/97JC02546 . _eprint: https://onlinelibrary.wiley.com/doi/pdf/10.1029/97JC02546. Accessed 2023-03-07

[27] Stein, K., Timmermann, A., Schneider, N., Jin, F.-F., Stuecker, M.F.: ENSO Seasonal Synchronization Theory. Journal of Climate **27**(14), 5285–5310 (2014) https://doi.org/10.1175/JCLI-D-13-00525.1 . Publisher: American Meteorological Society Section: Journal of Climate. Accessed 2023-03-07

[28] Chen, H.-C., Jin, F.-F.: Fundamental Behavior of ENSO Phase Locking. Journal of Climate **33**(5), 1953–1968 (2020) https://doi.org/10.1175/JCLI-D-19-0264.1 . Publisher: American Meteorological Society Section: Journal of Climate. Accessed 2023-03-07

[29] Kim, S.-K., An, S.-I.: Seasonal Gap Theory for ENSO Phase Locking. Journal of Climate **34**(14), 5621–5634 (2021) https://doi.org/10.1175/JCLI-D-20-0495.1 . Publisher: American Meteorological Society Section: Journal of Climate. Accessed 2023-02-01

[30] Chen, H.-C., Jin, F.-F.: Dynamics of ENSO Phase–Locking and Its Biases in Climate Models. Geophysical Research Letters **49**(3), 2021–097603 (2022) https://doi.org/10.1029/2021GL097603 . _eprint: https://onlinelibrary.wiley.com/doi/pdf/10.1029/2021GL097603. Accessed 2023-03-07

[31] Tziperman, E., Zebiak, S.E., Cane, M.A.: Mechanisms of Seasonal – ENSO Interaction. Journal of the Atmospheric Sciences **54**(1), 61–71 (1997) https://doi.org/10.1175/1520-0469(1997)054⟨0061:MOSEI⟩2.0.CO;2 . Publisher: American Meteorological Society Section: Journal of the Atmospheric Sciences. Accessed 2023-03-07

[32] Zebiak, S.E., Cane, M.A.: A Model El Ni&ntilde–Southern Oscillation. Monthly Weather Review **115**(10), 2262–2278 (1987) https://doi.org/10.1175/1520-0493(1987)115⟨2262:AMENO⟩2.0.CO;2 . Publisher: American Meteorological Society Section: Monthly Weather Review. Accessed 2023-04-19

[33] Vallis, G.K.: Conceptual models of El Niño and the Southern Oscillation. Journal of Geophysical Research: Oceans **93**(C11), 13979–13991 (1988) https://doi.org/10.1029/JC093iC11p13979 . _eprint: https://onlinelibrary.wiley.com/doi/pdf/10.1029/JC093iC11p13979. Accessed 2023-09-09

[34] Tuckman, P.J., Smyth, J., Lutsko, N.J., Marshall, J.: The Zonal Seasonal Cycle of Tropical Precipitation: Introducing the Indo-Pacific Monsoonal Mode. Journal of Climate **-1**(aop) (2024) https://doi.org/10.1175/JCLI-D-23-0125.1 . Publisher: American Meteorological Society Section: Journal of Climate. Accessed 2024-04-10

[35] Hersbach, H., Bell, B., Berrisford, P., Hirahara, S., Horányi, A., Muñoz-Sabater, J., Nicolas, J., Peubey, C., Radu, R., Schepers, D., Simmons, A., Soci, C., Abdalla, S., Abellan, X., Balsamo, G., Bechtold, P., Biavati, G., Bidlot, J., Bonavita, M., De Chiara, G., Dahlgren, P., Dee, D., Diamantakis, M., Dragani, R., Flemming, J., Forbes, R., Fuentes, M., Geer, A., Haimberger, L., Healy, S., Hogan, R.J., Hólm, E., Janisková, M., Keeley, S., Laloyaux, P., Lopez, P., Lupu, C., Radnoti, G., Rosnay, P., Rozum, I., Vamborg, F., Villaume, S., Thépaut, J.-N.: The ERA5 global reanalysis. Quarterly Journal of the Royal Meteorological Society **146**(730), 1999–2049 (2020) https://doi.org/10.1002/qj.3803 . _eprint: https://onlinelibrary.wiley.com/doi/pdf/10.1002/qj.3803. Accessed 2022-03-29

[36] Boos, W.R., Korty, R.L.: Regional energy budget control of the intertropical convergence zone and application to mid-Holocene rainfall. Nature Geoscience **9**(12), 892–897 (2016) https://doi.org/10.1038/ngeo2833 . Bandiera_abtest: a Cg_type: Nature Research Journals Number: 12 Primary_atype: Research Publisher: Nature Publishing Group Subject_term: Atmospheric dynamics;Climate and Earth system modelling;Palaeoclimate Subject_term_id: atmospheric-dynamics;climate-and-earth-system-modelling;palaeoclimate. Accessed 2021-06-23

[37] Bjerknes, J.: ATMOSPHERIC TELECONNECTIONS FROM THE EQUATORIAL PACIFIC. Monthly Weather Review **97**(3), 163–172 (1969) https://doi.org/10.1175/1520-0493(1969)097⟨0163:ATFTEP⟩2.3.CO;2 . Publisher: American Meteorological Society Section: Monthly Weather Review. Accessed 2023-06-29

[38] Takahashi, K., Battisti, D.S.: Processes Controlling the Mean Tropical Pacific Precipitation Pattern. Part I: The Andes and the Eastern Pacific ITCZ. Journal of Climate **20**(14), 3434–3451 (2007) https://doi.org/10.1175/JCLI4198.1 . Publisher: American Meteorological Society Section: Journal of Climate. Accessed 2023-04-22

[39] Takahashi, K., Battisti, D.S.: Processes Controlling the Mean Tropical Pacific Precipitation Pattern. Part II: The SPCZ and the Southeast Pacific Dry Zone. Journal of Climate **20**(23), 5696–5706 (2007) https://doi.org/10.1175/2007JCLI1656.1 . Publisher: American Meteorological Society Section: Journal of Climate. Accessed 2023-04-22

[40] Baldwin, J.W., Atwood, A.R., Vecchi, G.A., Battisti, D.S.: Outsize Influence of Central American Orography on Global Climate. AGU Advances **2**(2), 2020–000343 (2021) https://doi.org/10.1029/2020AV000343 . _eprint: https://onlinelibrary.wiley.com/doi/pdf/10.1029/2020AV000343. Accessed 2023-05-15

[41] Marshall, J., Donohoe, A., Ferreira, D., McGee, D.: The ocean's role in setting the mean position of the Inter-Tropical Convergence Zone. Climate Dynamics **42**(7), 1967–1979 (2014) https://doi.org/10.1007/s00382-013-1767-z . Company: Springer Distributor: Springer Institution: Springer Label: Springer Number: 7 Publisher: Springer Berlin Heidelberg. Accessed 2020-09-24

[42] Lu, Z., Liu, Z.: Orbital modulation of ENSO seasonal phase locking. Climate Dynamics **52**(7), 4329–4350 (2019) https://doi.org/10.1007/s00382-018-4382-1 . Accessed 2023-11-30

[43] Li, T., Philander, S.G.H.: On the Annual Cycle of the Eastern Equatorial Pacific. Journal of Climate **9**(12), 2986–2998 (1996). Publisher: American Meteorological Society. Accessed 2023-02-27

[44] Philander, S.G.H., Gu, D., Lambert, G., Li, T., Halpern, D., Lau, N.-C., Pacanowski, R.C.: Why the ITCZ Is Mostly North of the Equator. Journal of Climate **9**(12), 2958–2972 (1996) https://doi.org/10.1175/1520-0442(1996)009⟨2958:WTIIMN⟩2.0.CO;2 . Publisher: American Meteorological Society Section: Journal of Climate. Accessed 2023-02-27

[45] Bellenger, H., Guilyardi, E., Leloup, J., Lengaigne, M., Vialard, J.: ENSO representation in climate models: from CMIP3 to CMIP5. Climate Dynamics **42**(7), 1999–2018 (2014) https://doi.org/10.1007/s00382-013-1783-z . Accessed 2024-04-26

[46] Tian, B., Ren, H.-L., Jin, F.-F., Stuecker, M.F.: Diagnosing the representation and causes of the ENSO persistence barrier in CMIP5 simulations. Climate Dynamics **53**(3), 2147–2160 (2019) https://doi.org/10.1007/s00382-019-04810-4 . Accessed 2024-04-26

[47] Liu, M., Ren, H.-L., Zhang, R., Ineson, S., Wang, R.: ENSO phase-locking behavior in climate models: from CMIP5 to CMIP6. Environmental Research Communications **3**(3), 031004 (2021) https://doi.org/10.1088/2515-7620/abf295 . Publisher: IOP Publishing. Accessed 2024-04-26

[48] Duan, W., Wei, C.: The 'spring predictability barrier' for ENSO predictions and its possible mechanism: results from a fully coupled model. International Journal of Climatology **33**(5), 1280–1292 (2013) https://doi.org/10.1002/joc.3513 . _eprint: https://onlinelibrary.wiley.com/doi/pdf/10.1002/joc.3513. Accessed 2023-03-13

[49] Levine, A.F.Z., McPhaden, M.J.: The annual cycle in ENSO growth rate as a cause of the spring predictability barrier. Geophysical Research Letters **42**(12), 5034–5041 (2015) https://doi.org/10.1002/2015GL064309 . _eprint: https://onlinelibrary.wiley.com/doi/pdf/10.1002/2015GL064309. Accessed 2023-03-13

[50] Webster, P.J., Yang, S.: Monsoon and Enso: Selectively Interactive Systems. Quarterly Journal of the Royal Meteorological Society **118**(507), 877–926 (1992) https://doi.org/10.1002/qj.49711850705 . _eprint: https://onlinelibrary.wiley.com/doi/pdf/10.1002/qj.49711850705. Accessed 2023-05-08

[51] Marshall, J., Adcroft, A., Hill, C., Perelman, L., Heisey, C.: A finite-volume, incompressible Navier Stokes model for studies of the ocean on parallel computers. Journal of Geophysical Research: Oceans **102**(C3), 5753–5766 (1997) https://doi.org/10.1029/96JC02775 . _eprint: https://onlinelibrary.wiley.com/doi/pdf/10.1029/96JC02775. Accessed 2022-03-17

[52] Adcroft, A., Campin, J.-M., Hill, C., Marshall, J.: Implementation of an Atmosphere–Ocean General Circulation Model on the Expanded Spherical Cube. Monthly Weather Review **132**(12), 2845–2863 (2004) https://doi.org/10.1175/MWR2823.1 . Publisher: American Meteorological Society Section: Monthly Weather Review. Accessed 2022-03-21

[53] Frierson, D.M.W., Held, I.M., Zurita-Gotor, P.: A Gray-Radiation Aquaplanet Moist GCM. Part II: Energy Transports in Altered Climates. Journal of the Atmospheric Sciences **64**(5), 1680–1693 (2007) https://doi.org/10.1175/JAS3913.1 . Publisher: American Meteorological Society Section: Journal of the Atmospheric Sciences. Accessed 2022-03-21

[54] Byrne, M.P., O'Gorman, P.A.: Land–Ocean Warming Contrast over a Wide Range of Climates: Convective Quasi-Equilibrium Theory and Idealized Simulations. Journal of Climate **26**(12), 4000–4016 (2013) https://doi.org/10.1175/JCLI-D-12-00262.1 . Publisher: American Meteorological Society Section: Journal of Climate. Accessed 2022-03-21

[55] Gaspar, P., Grégoris, Y., Lefevre, J.-M.: A simple eddy kinetic energy model for simulations of the oceanic vertical mixing: Tests at station Papa and long-term upper ocean study site. Journal of Geophysical Research: Oceans **95**(C9), 16179–16193 (1990) https://doi.org/10.1029/JC095iC09p16179 . _eprint: https://onlinelibrary.wiley.com/doi/pdf/10.1029/JC095iC09p16179. Accessed 2023-04-24

[56] Mayer, J., Mayer, M., Haimberger, L.: Mass-consistent Atmospheric Energy and Moisture

Budget Data from 1979 to Present Derived from ERA5 Reanalysis, V1.0, Copernicus Climate Change Service (C3S) Climate Data Store (CDS). https://doi.org/10.24381/cds.c2451f6b Accessed 2022-09-14

[57] An, S.-I., Jin, F.-F.: Nonlinearity and Asymmetry of ENSO. Journal of Climate **17**(12), 2399–2412 (2004) https://doi.org/10.1175/1520-0442(2004)017⟨2399:NAAOE⟩2.0.CO;2 . Publisher: American Meteorological Society Section: Journal of Climate. Accessed 2023-08-18